ISSN (Print) 1226-1750
ISSN (Online) 2233-6656
Journal of Magnetics 23(2), 267-273 (2018) https://doi.org/10.4283/JMAG.2018.23.2.267

Characteristic Analysis of Interior Permanent Magnet Synchronous Machine by considering Magnetization Patterns

Ja-Hyeong Lee and Yu-Seop Park*

Department of Electrical Engineering, Korea National University of Transportation, Chungju 27469, Korea

(Received 2 March 2018, Received in final form 23 June 2018, Accepted 25 June 2018)

This paper deals with the comparative investigation on the electromagnetic field characteristics of interior permanent magnet synchronous motors (IPMSMs) based on finite element method. With identical magnetic structure, this paper proposes newly designed PM magnetization patterns for the cogging torque reduction. Based on this method, in spite of the longer stack length of the rotor and stator core, the torque characteristics can be much more improved in comparison with the conventional model. Along with the torque characteristics, the performance evaluation is also addressed based on the analyzed power loss values.

Keywords : Cogging Torque, IPMSM, Magnetization Pattern

1. Introduction

Permanent magnet synchronous motor (PMSM) has relatively higher efficiency and output power density in comparison with other types of motors without using PMs, so it is widely applied in various industrial applications. In the design of PMSM, according to the PM position, it can be largely categorized by the surface-mounted PMSM (SPMSM) and interior PMSM (IPMSM). Differently from the SPMSM, the IPMSM has small magnetic air-gap and higher energy density by using the additional reluctance torque [1]. However, its cogging torque and torque ripple due to the magnetic structure can cause the noise and vibration of its entire system. Therefore, their reduction is very important design objective. So far, in the previous literatures, the efforts on the improvement of torque were presented, such as skew structure [2], stator core design [3] and PM arrangement [4], and they became very popular method for motor designers. On the other hand, in this paper, by variation of PM magnetization patterns, the novel design of IPMSM is proposed, and it is very useful for the manufacturing cost reduction. For the substitution of the conventional model, the electromagnetic field characteristics including torque and power losses will be comparatively investigated.

*Corresponding author: Tel: +82-43-841-5148
Fax: +82-43-841-5140, e-mail: yspark@ut.ac.kr

2. Electromagnetic Field Analysis by considering PM Magnetization Patterns based on FEM

2.1. Analysis Model

First of all, since the main objective of this study is to design the alternative machine, the objective functions and design variables with constraints are presented in Table 1. As can be confirmed in the table, the alternative model is required to minimize the cogging torque and total harmonic distortion (THD) of induced voltage. However, since we have to use the original stator and rotor core, only the PM and the stack length can be determined as design variables. Here, as constraints, the induced voltage in *rms* value and the average torque of the original model and the newly designed model should be identical.

Table 1. Design Requirements.

Objective Functions	
- Minimization of cogging torque	
- Minimization of THD of induced voltage for torque ripple reduction	
Design Variables	
- Magnetization	Forward / Reverse
- Length of PM width	3.4 (mm) < L_{PM} < 7.4 (mm)
- Stack length	50 (mm) < L_{stack} < 100 (mm)
Constraints	
- Identical induced voltage and average torque	

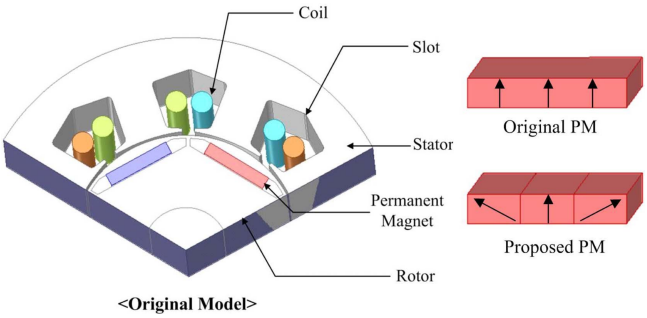

Fig. 1. (Color online) Analysis model of original IPMSM with 6 poles and 9 slots.

Table 2. Design Specification of Analysis Model.

Specification	Value	Specification	Value
Rated Speed	2,500 (rpm)	Rated Torque	0.55 (Nm)
Rated Power	143.3 (W)	Rated Current	1.5 (A)
Outer Dia. of rotor	54.0 (mm)	Outer Dia. of stator	100.0 (mm)
Stack Length	55.0 (mm)	Number of Poles	6
Number of Slots	9	Number of Turns	84
Core Material	35PN230	Air-gap Length	0.5 (mm)
Cooling Method	Natural	Coil Size	AWG 24
Parallel Branch	1	Br of PM at 60 (°C)	1.24 (T)

Fig. 1 shows the magnetic structure of IPMSM addressed in this paper. It has 6 poles in rotor with 9 slots in stator, and the NdFeB PMs, which are rare-earth material, are employed while the 3-phase concentrated winding is placed in the stator.

More detailed design specifications are presented in Table 2. In addition, as can be confirmed in Fig. 2, the rated speed is 2,500 (rpm). Until the maximum speed of 5,000 (rpm), operating range is largely divided by the constant torque region and the constant power region based on the rated speed. Here, the proper combination of d-axis and q-axis current is employed for the field weakening control in the constant power region. As it is well known, the torque can be expressed as (1), and it is composed of magnetic torque and reluctance torque, so the relatively higher torque can be achieved by using the proper d-axis current [1].

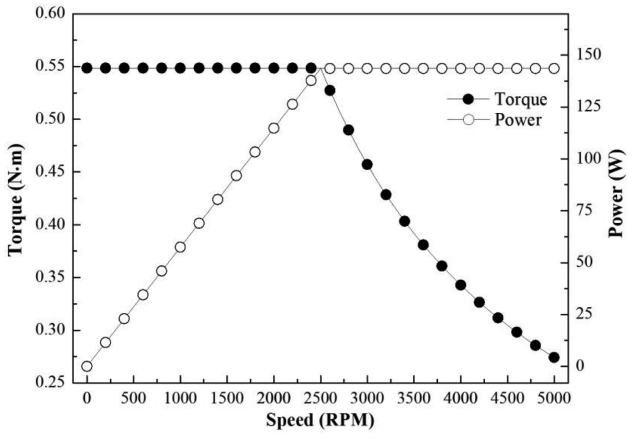

Fig. 2. Torque and power curve versus rotational speed.

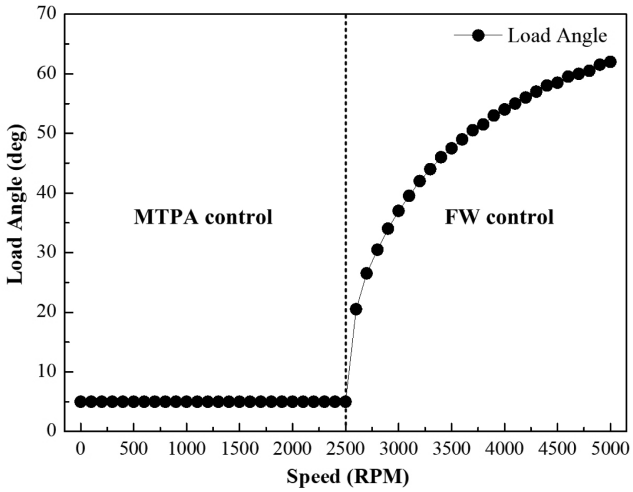

Fig. 3. Load angle of current MTPA and FW control.

$$T = \frac{3}{2} p \left(\lambda_{PM} I_a \cos\beta + \frac{1}{2}(L_q - L_d) I_a{}^2 \sin 2\beta \right) \quad (1)$$

Here, p is number of pole pairs, L_d and L_q are d-axis inductance and q-axis inductance, and β is current phase angle. In the torque equation, the first term on the right side is called as magnetic torque and the second term is called as reluctance torque.

Figure 3 shows the load angle according to the rotational speed of the analysis model, and the current vector trajectory of the motor is determined according to the maximum torque per ampere (MTPA) and field weakening (FW) control for constant torque region and constant power region. The analysis model covered in this paper has a rated current of 1.5(A) in rms value as can be confirmed in Table 1.

On the other hand, as presented in Fig. 1, the analysis model has six PMs inserted in six slots of the rotor core. It is well known that eddy current loss occurs on the surface of the PMs during high-speed operation. Therefore, in the previous literatures, attractive solution has been proposed to reduce the loss by dividing the magnets [5]. When the magnets are divided, we could have more design options for the magnetization direction of the PMs, and the cogging torque characteristic of the analytical model can be improved.

2.2. Magnetization of segmented PMs

As presented in [6], the cogging torque of IPMSM is

generated by rotor position and flux density in air-gap change as shown in (2) and (3). Here, α means the rotor position angle, and θ denotes the circumferential direction. $B_r(\theta)$ represents the radial component of the flux density of the PM. Lastly, h_m is length of the magnetization direction, g is length of the gap.

$$T_{cog} = -\frac{\partial W}{\partial \alpha} \tag{2}$$

$$W = \frac{1}{2\mu_0}\int_V B_r^{\,2}(\theta)\left(\frac{h_m(\theta)}{h_m(\theta)+g(\theta,\alpha)}\right)^2 dV \tag{3}$$

This is a result of the magnetic structure of the rotor and the stator including the PMs, and it can be reduced through various methods as mentioned above. However, in this study, the direction of magnetization is directly changed to improve the THD of the no-load induced voltage and to reduce the cogging torque. In the other words, a design method is applied in which a magnet is divided into three parts from an existing PM, and the direction of magnetization is made different for each permanent magnet.

The permanent magnet applied in this paper is the rare earth series N42SH, which shows the BH curve of the permanent magnet according to temperature in Fig. 4. In this paper, the operating temperature of the motor is selected as 60 (ºC). As can be seen in the figure, there exists a knee point which causes irreversible magnetization of the permanent magnet under the condition of about 780 (kA/m) at 100 (°C). However, since it is not greatly influenced by the external magnetic field at 60 (°C), Therefore, the possibility that it may happen during its operation is very low.

Figure 5 shows the design changes of the three PMs applied from the existing model, which are defined as

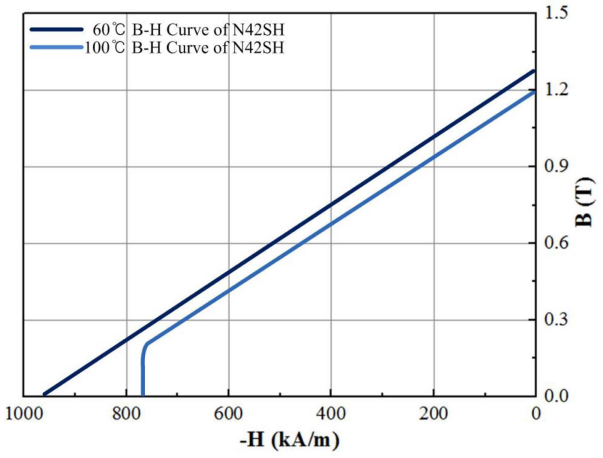

Fig. 4. (Color online) BH curve of permanent magnet according to temperature (N42SH).

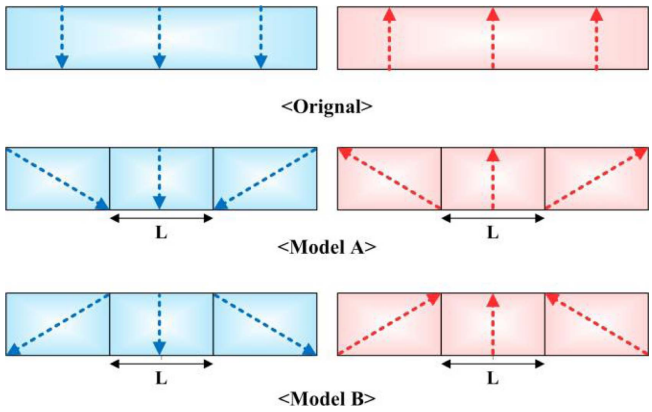

Fig. 5. (Color online) Permanent magnet design by applying length variation of 3 segments based on original model.

Model A and Model B. Here, the magnetization direction of the PM is indicated by arrows, and the width of the central portion of the three divided PMs is defined as L. It will be shown that the width ratio of the divided magnets have high influence on the electromagnetic characteristics.

2.3. Open Circuit Field

Figure 6 shows the results of the electromagnetic characteristics analysis of Model A and B based on the FEM. Figure 6(a) shows that the value of model B is smaller than that of Model A as a result of cogging torque analysis. Especially when the width of three PMs divided in model B is almost equal (As L approaches 5.4 mm), it can be seen that the cogging torque decreases gradually. On the basis of minimum value of each model, the model A is 63.8 (Nm), the model B is 18.18 (Nm). As a result, the model B shows smaller values of 71.5 (%). In addition, Fig. 6(b) and Fig. 6(c) respectively present the no-load induced voltage and THD of Model A and Model B. Here, the THD is calculated by (4). Here, V_1 is the fundamental value, and n is the harmonic order.

$$THD = \frac{\sqrt{\sum_{n\neq 1}^{\infty} V_n^2}}{V_1} \tag{4}$$

As can be confirmed in the figure, very similar patterns were achieved from the induced voltage of both models with a bit little higher values in Model B. On the contrary to the induced voltage in no-load condition, the THD shows opposite trend. In other words, the decreasing values of THD are analyzed while the L reaches to 5.4(mm), but Model B shows the highest value in the identical condition.

However, Model B presents entirely lower values in comparison of Model A, and the difference of the THD

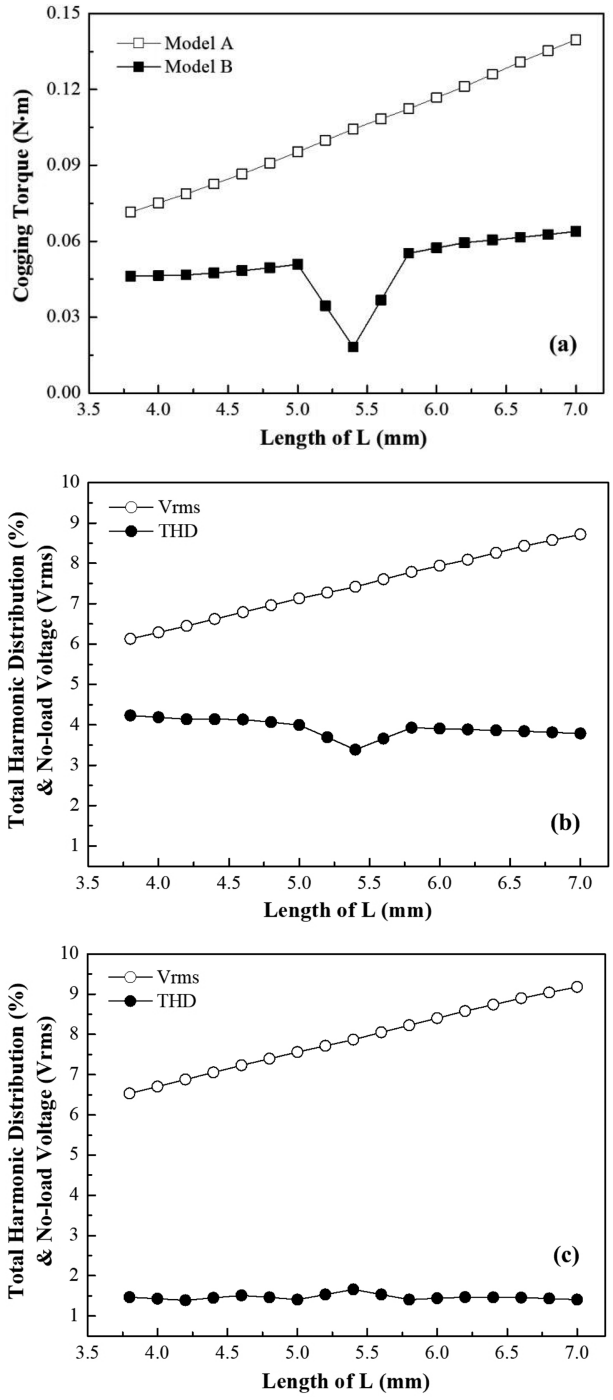

Fig. 6. No-load characteristics according to magnetization patterns: (a) Cogging torque, (b) no-load induced voltage and its THD of model A, (c) no-load induced voltage and its THD of model B.

values in each condition is minor, so it can be concluded that the Model B has superior characteristic to Model A.

On the other hand, Table 3 compares the analyzed results according to the magnetization pattern and the stack length. As can be seen in the table, it can be confirmed that the induced voltage of the model B is reduced as compared with the model A. This is due to the reduction of the magnetic flux density in air-gap. For the better understanding, the radial and tangential components of the magnetic flux density in air-gap for each model are calculated by (5) and (6), respectively. In particular, from Fig. 7(a), it can be confirmed that the results of the radial component are very different. The peak value of proposed model is 39 (%) less than that of the original model.

Table 3. Comparative Results in Open Circuit Field.

	Stack Length (mm)	No-load Voltage (V)	Total Harmonic Distortion (%)	Cogging Torque (Nm)
Original	55	12.68	2.33	0.187
Model A	55	7.41	3.38	0.104
Model B	55	7.86	1.66	0.018
Proposed model	88.6	12.67	1.66	0.029

$$B_r = B_x \cos(\theta) + B_y \sin(\theta) \tag{5}$$

$$B_t = -B_x \sin(\theta) + B_y \cos(\theta) \tag{6}$$

So, for reasonable comparison, the axial length to satisfy the induced voltage of the Model A was designed as 88.6 (mm), Therefore, we can confirm THD and cogging torque are greatly improved under the same condition.

In addition, Fig. 8 shows half of the electrical cycle of cogging torque from both models, and the three periods can be calculated by (7). Here, *LCM* means the least common multiple while *pole* and *slot* indicates the number of poles and slots, respectively.

$$K_{cogging} = LCM(pole, slot) / pole \tag{7}$$

2.4. Load Characteristics considering Electrical Power Loss

The losses of the IPMSM can be divided into electrical loss such as copper loss, iron loss, rotor loss and mechanical loss such as friction loss and windage loss as shown in Fig. 9 [7].

Since the analysis models dealt with in this paper are relatively low-speed machines, the performance of the motor is evaluated by comparing electrical losses without considering mechanical losses. At first, copper loss can be derived from the controlled stator current and the calculated resistance with (8), assuming that the stator windings of the three phases are identical.

$$P_{cu} = 3R_s \left(i_d^{e^2} + i_q^{e^2} \right) / 2 \tag{8}$$

Also, the iron loss explained by (9) can be calculated as

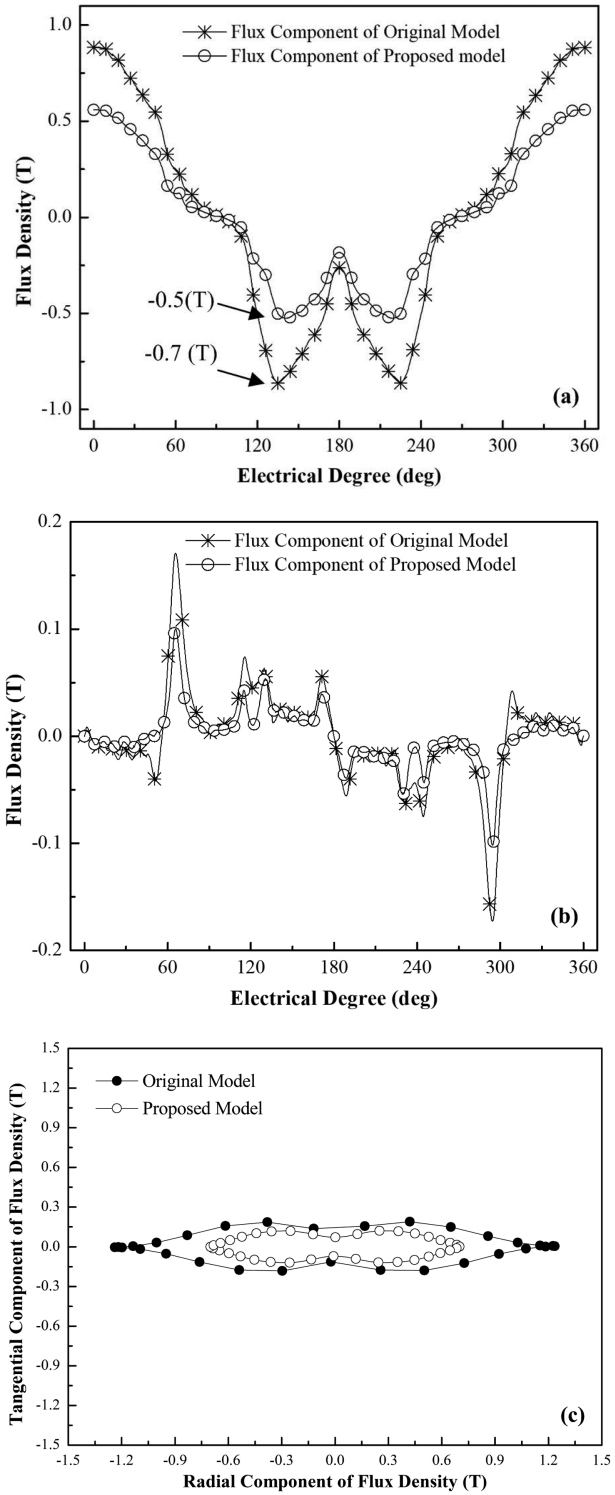

Fig. 7. Comparison the air gap flux density of analysis models: (a) Radial component, (b) Tangential component, (c) magnetic behavior in stator tooth.

the sum of hysteresis loss and eddy current loss. As mentioned before, we employed 35PN230 from POSCO, and the coefficient of hysteresis loss and eddy current loss

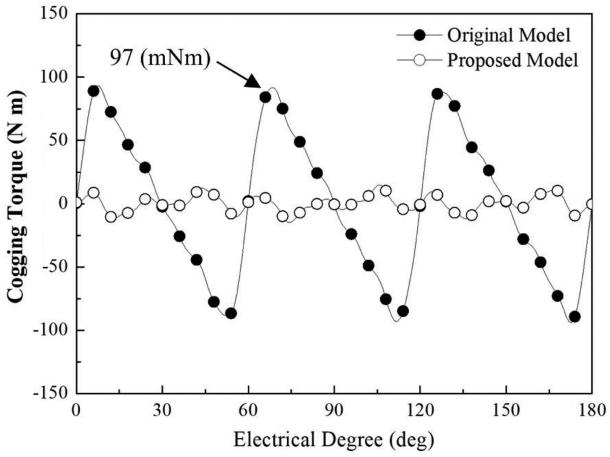

Fig. 8. Analysis result of cogging torque between model according to half period of electrical degree.

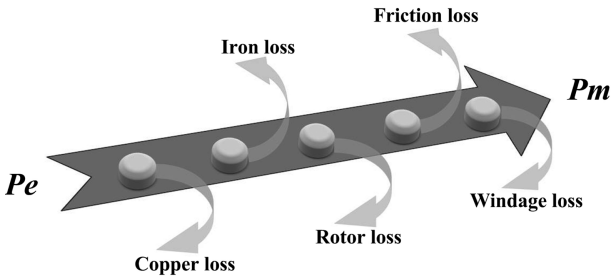

Fig. 9. Energy flow of IPMSM considering power losses.

are 293.4 and 0.558, respectively.

$$P_{core} = \sum_{l=1,odd}^{\infty} Q_1 \left(K_{hl} f_l B_l^n + K_{el} f_l^2 B_l^2 \right) \tag{9}$$

Besides, the eddy current loss on the PM surface was derived by FEM considering the conductivity of the PM as 625,000 (S/m).

Figure 10 compares the losses for each model calculated at the rated speed of 2,500 (rpm) and the current of 1.5 (A_{rms}). As mentioned above, since the stator resistance is designed to be identical, the values of the copper loss are very similar. Besides, for the cases of iron and rotor losses, the proposed model is superior to original model. This is the result from the lower flux density for core loss and from the divided PMs for rotor loss. On the other hand, when evaluating the performance of the motor, torque ripple which can have high influence on the vibration and noise is also very important design consideration. Figure 11 compares the torque ripple of each model when rated speed and output in operating condition shown in Fig. 2. It shows that the torque ripple as well as the cogging torque and the electromagnetic losses is improved. In addition, under the identical volume condi-

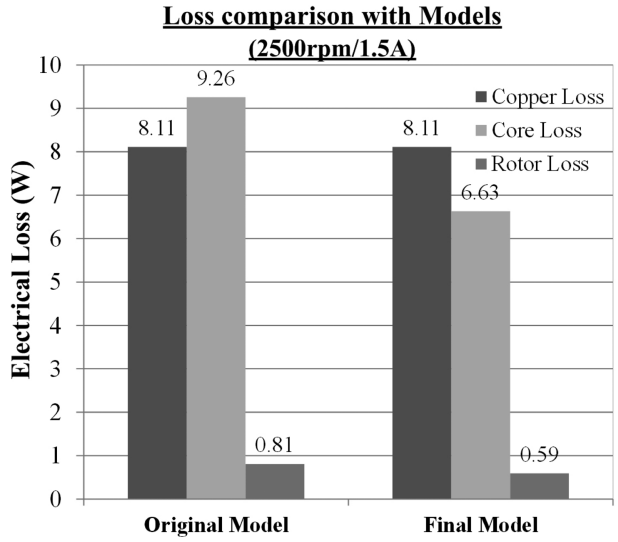

Fig. 10. Each loss of analysis models at rated speed (2,500 rpm) and current (1.5 A) condition.

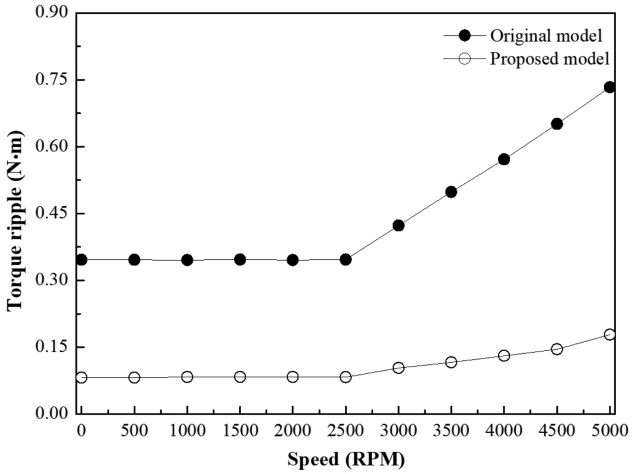

Fig. 11. Comparison torque ripple of original and proposed model.

tion of permanent magnets, the torque density of the newly designed model is calculated as 732.9 (mNm/m^2) while that of the original model is calculated as 1259.3 (mNm/m^2) in 1.5(A) condition.

2.5. Experimental verification

The proposed PM motor applied the magnetization direction is not manufactured yet, so its experiment could not be performed. However, since the validity of the FEM is very well known, the comparison between the experimental result and the analyzed value of the original model can be an alternative way.

Consequently, the experimental set was constructed as shown in Fig. 12 with an operating motor and an inverter

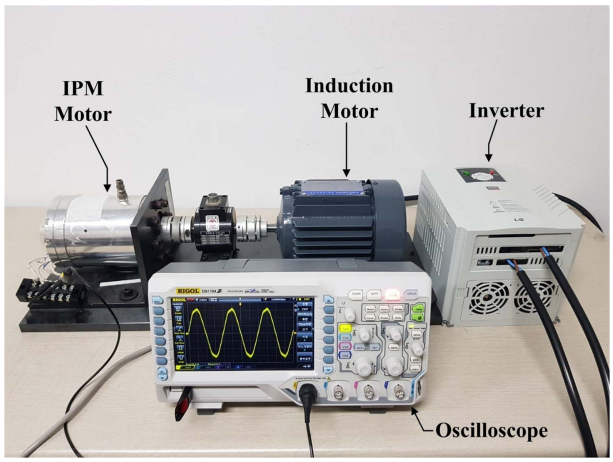

Fig. 12. (Color online) Experimental set-up construction with operating motor and inverter to measure induced voltage in no-load condition (line-to-line).

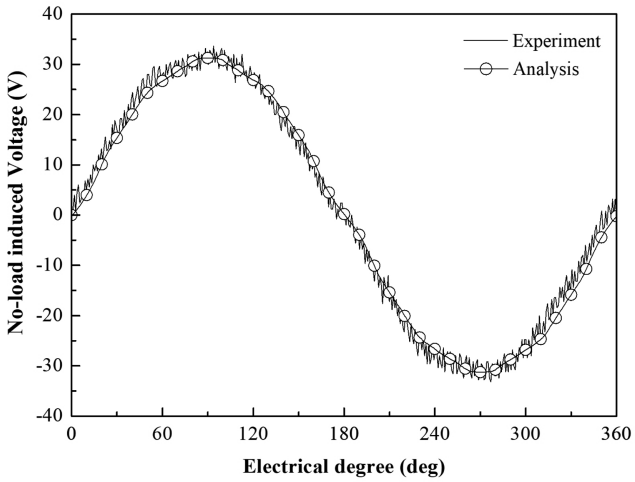

Fig. 13. Comparison of no-load induced voltage of analysis result and measured waveform (1,000 rpm).

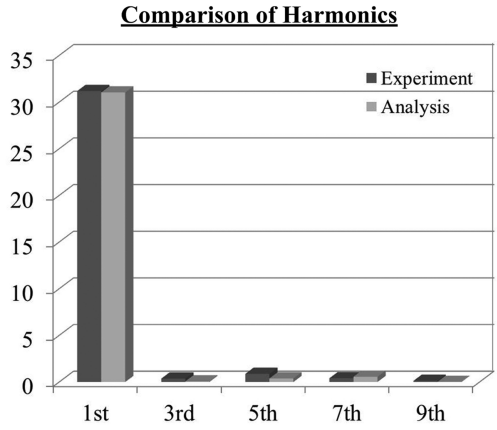

Fig. 14. Comparison of Harmonics of analysis result and measured (1,000 rpm).

with a measuring instrument. Here, the line-to-line voltage is measured in 1,000 (rpm) of rotating speed condition. Figure 13 and Fig. 14 compare the analyzed value with the measured one, and it can be confirm that the results are very well corresponded.

3. Conclusion

In this paper, the electromagnetic characteristics of IPMSM through FEM are analyzed, and a newly designed machine is proposed for performance improvement. The cogging torque is reduced by the designed magnetization pattern with divided PMs while the magnetic structures of original model, such as stator core and rotor core, are not varied.

In addition, not only is the torque ripple which can have influence on the vibration and noise of the motor improved, but also the electrical power losses are reduced. On the other hand, the validity of the analysis procedure and design presented in this paper is verified through experiments, so it can be one of the useful references for its related industrial area.

Acknowledgment

This was supported by Korea National University of Transportation in 2018, and this work was supported by the National Research Foundation of Korea (NRF) grant funded by the Korea government (MSIP; Ministry of Science, ICT & Future Planning) (No. 2017R1C1B5015907).

References

[1] W. H. Kim, M. J. Kim, K. D. Lee, J. J. Lee, J. H. Han, T. C. Jeong, S. Y. Cho, and J. Lee, IEEE Trans. Magn. **50**, 4001404 (2013).
[2] W. Zhao, T. A. Lipo, and B. I. Kwon, IEEE Trans. Magn. **51**, 8110804 (2015).
[3] J. S. Choi, K. Izui, S. Nishiwaki, A. Kawamoto, and T. Nomura, IEEE Trans. Magn. **47**, 3024 (2011).
[4] S. H. Lim, S. J. Min, and J. P. Hong, IEEE Trans. Magn. **51**, 8202405 (2015).
[5] Y. Hu, S. Zhu, and C. Liu, IEEE Trans. Magn. **53**, 7402904 (2017).
[6] D. W. Wang, X. Wang, M. K. Kim, and S. Y. Jung, IEEE Trans. Magn. **48**, 2265 (2012).
[7] K. J. Ko, S. M. Jang, J. H. Park, H. W. Cho, and D. J. You, IEEE Trans. Magn. **47**, 3292 (2011).